Appl. Phys. A 80, 51–54 (2005)
DOI: 10.1007/s00339-004-3013-3

Applied Physics A
Materials Science & Processing

R.-A. EICHEL[1,✉]
K.-P. DINSE[1]
H. KUNGL[2]
M.J. HOFFMANN[2]
A. OZAROWSKI[3]
J. VAN TOL[3]
L.C. BRUNEL[3]

Exploring the morphotropic phase boundary in copper(II)-modified $Pb[Zr_{0.54}Ti_{0.46}]O_3$ ferroelectrics

[1] Eduard-Zintl-Institute, Darmstadt University of Technology, 64287 Darmstadt, Germany
[2] Institute of Ceramics in Mechanical Engineering, University of Karlsruhe, 76131 Karlsruhe, Germany
[3] Center for Interdisciplinary Magnetic Resonance, National High Magnetic Field Laboratory, Florida State University, Tallahassee, FL 32310, USA

Received: 24 June 2004/Accepted: 22 July 2004
Published online: 14 September 2004 •

ABSTRACT Copper(II)-doped $Pb[Zr_{0.54}Ti_{0.46}]O_3$ (PZT) ferroelectrics with a dopant concentration of 0.25 mol % were investigated at high magnetic fields, enabling an enhanced resolution of the structural distortion at the dopant site. The results obtained suggest that Cu^{2+} substitutes as an acceptor centre for $[Zr, Ti]^{4+}$ in oxygen octahedra with tetragonal, monoclinic and rhombohedral distortion, confirming the model of mesoscopic mixing at the morphotropic phase boundary.

PACS 61.72.Ji; 61.72.Ww; 76.30.Fc; 77.80.Bh; 77.84.Dy

1 Introduction

Perovskite-type zirconate titanate oxides $Pb[Zr_xTi_{1-x}]O_3$ (PZT $x/1-x$) are commercially the most important piezoelectric materials for sensor and actuator applications, because of their superior properties and notably due to the ability of tailoring these properties by doping with aliovalent ions. Hence, considerable interest exists in the role of dopant ions, where already small concentrations have strong impact on PZT ferro- and piezoelectric properties. In particular, compounds with Zr/Ti ratios near the morphotropic phase boundary (MPB) exhibit extremely high electromechanical coupling due to the coexistence of rhombohedral Zr-rich and tetragonal Ti-rich phases [1, 2]. Recently, it has been proposed that a monoclinic phase at the MPB, as a subgroup of both structures, can build a bridge between these phases, favouring a polarization rotation [3–5]. However, electron-microscopy studies have reported the presence of small domains with ordered cation displacements that cannot be explained in terms of the proposed average monoclinic structure [6–8]. In another picture, the MPB consists of an 'average structure' due to a statistical distribution of Zr- and Ti-rich environments with corresponding tetragonal and rhombohedral phases [9].

Whereas X-ray diffraction techniques are based upon coherent scattering at extended crystallographic planes and therefore are insensitive to subtle short-range changes as induced by small amounts of dopants, electron paramagnetic resonance (EPR) can often determine the configuration of the incorporated impurity and yields local structure information at particular dopant sites. Single-crystal EPR has been performed on copper-doped $PbTiO_3$, finding a single copper centre of axial symmetry, the observed g values being consistent with a coordination at the Ti site [10]. In polycrystalline ceramics like $Cu:[Pb_yLa_{1-y}]TiO_3$, a single axial centre with $g_\parallel > g_\perp > g_e$ was found in accordance with the tetragonal crystal structure [11]. For the solid-solution system $Cu:Pb[Zr_xTi_{1-x}]O_3$ with various compositions x ranging from 0 to 0.9, the Cu^{2+} ion was proposed to be situated in two different environments, one with $g_\parallel > g_\perp > g_e$ and the other with $g_\perp > g_\parallel > g_e$ [12]. The sign change of the g-matrix anisotropy was rationalized by assuming the formation of a tetragonally compressed octahedron. It was argued that the addition of Zr to the lattice causes increased distortion at the B-site, thus being responsible for this deformation. EPR was also employed in copper-doped electro-optic $[Pb_{0.92}La_{0.08}][Zr_{0.65}Ti_{0.35}]O_3$ (PLZT 8/65/35) ceramics [13], in which the observed EPR spectra were simulated by a superposition of axial and isotropic Cu^{2+} spectra of unknown origin. In $Cu:BaTiO_3$ ceramics, two superposed copper centres were also observed [14]. Depending on doping level and sintering temperature, the EPR data exhibited two different Cu^{2+}_{Ti} spectra with $g_\parallel > g_\perp > g_e$ in both cases, attributed to tetragonally distorted CuO_6 octahedra in tetragonal and rhombohedral crystal surroundings, respectively.

Obviously, the exact nature of the structural role of Cu^{2+} ions and the associated oxygen vacancies in PZT ceramics remains ambiguous. In this work, high-field EPR at 94 GHz (W-band) and 240 GHz was employed. The main rationale for this high-field analysis is first to critically review the proposed existence of two different copper centres [12], and second to discriminate between the two proposed structural models for the MPB. For both purposes the inherent enhanced ability to resolve small g-value differences at high fields is exploited. 10-GHz (X-band) EPR experiments used predominantly up to now were not able to answer these questions unambiguously because of the presence of a large anisotropic copper hyperfine interaction, preventing the definite assignment of the corresponding g values.

2 Experimental

Powder samples studied were prepared as described earlier [15] and characterized as a mixture of tetrago-

✉ Fax: +49-6151-16-43-47, E-mail: eichel@chemie.tu-darmstadt.de

nal and rhombohedral perovskite phases at ambient temperature. No presence of lead oxide or lead titanate secondary phases was detected.

The spectroscopic W-band pulse EPR measurements were performed on a Bruker ElexSys 680 spectrometer, using a cylindrical TE_{011} flexline resonator (Bruker). As field marker, the background signals from Mn(II) with $g = 2.002$ were used for magnetic field calibration. Echo-induced EPR spectra were recorded as a function of the external field by integrating over the echo that follows two selective microwave (mw) pulses of 150-ns duration and an interpulse delay of 500 ns.

Field-modulated continuous-wave 240-GHz EPR experiments were performed at the high magnetic field facility at the National High Magnetic Field Laboratory [16]. Detection was provided with a low-noise, wide-frequency-range InSb hot-electron bolometer (QMC Ltd.), operated at liquid-helium temperature. Microwave radiation was provided by a quartz synthesizer. No resonator was used.

3 Theoretical description

The spin Hamiltonian for an unpaired $3d^9$ electron with spin $S = \frac{1}{2}$ can be written as

$$\mathcal{H} = \beta_e B_0\, g\, S - \beta_n g_n B_0\, I + S\, A\, I, \qquad (1)$$

where g_n is the corresponding nuclear g factor and β_e and β_n are the Bohr and nuclear magnetons, respectively. The first and second terms represent the electronic and nuclear Zeeman interactions, respectively, where B_0 denotes the external field, given in the principal axes system of the g tensor. The last term is due to the copper hyperfine interaction $\left(I^{(Cu)} = \frac{3}{2}\right)$ that was not resolved in the spectra and at high fields primarily leads to line broadening. The nuclear quadrupole interaction does not contribute in first approximation to the EPR spectra and thus has been neglected. Numerical simulations of the spectra were based on the spin Hamiltonian (1), including g and A strains modelled as Gaussian distributions of the corresponding parameters.

4 Results and discussion

In the echo-induced W-band EPR spectrum of 0.25 mol %-doped Cu:PZT 54/46 at 5 K, shown in Fig. 1, a much simpler spectrum with enhanced g-matrix resolution results as compared to the X-band spectrum [15]. On the other hand, the hyperfine features are lost since this interaction does not scale linearly with the field, whereas the inhomogeneous broadening increases because of g strain. The obtained g values are listed in Table 1.

Two numerical simulations using the spin Hamiltonian (1) are superimposed to the experimental spectrum. One simulation (dashed) uses the parameters proposed in [12], invoking two copper centres, and the other simulation invokes instead a single g matrix of axial symmetry (dotted). The remaining spectral features originate from a Mn(II) spin marker calibrating the magnetic field (marked by an asterisk). Obviously, the obtained W-band EPR spectrum gives clear evidence that there is no second copper centre with an inverted sequence of pseudo-axial g-matrix parameters. We therefore can rule out the existence of an additional tetragonally compressed CuO_6 octahedron.

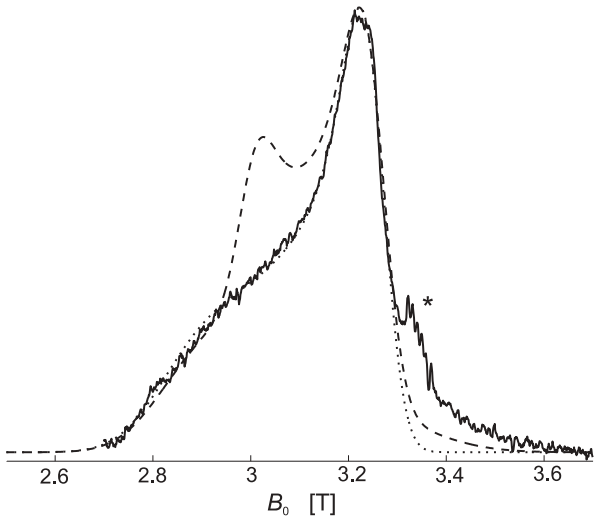

FIGURE 1 High-field EPR of 0.25 mol %-doped Cu:PZT 54/46 at W-band ($\nu_{mw} = 94.116$ GHz) and 5 K. Superimposed to the experimental spectrum, two numerical simulations using the spin Hamiltonian (1) are displayed, in which one simulation (*dashed*) uses the parameters proposed in [12], invoking two different copper centres, and the other simulation uses a single g matrix with axial (*dotted*) symmetry. The Mn(II) spin marker is indicated by an *asterisk*

The observed $g_\parallel$ and $g_\perp$ values are characteristic of Cu^{2+} coordinated by six ligands that form an octahedron elongated by tetragonal distortion along the z axis [17]. Good agreement is obtained with values reported for similar compounds (cf. Table 1). These can be understood in terms of a five-fold orbital degeneracy of a $3d^9$ ion that is split in the presence of an octahedral crystal field into a triplet (t_{2g}) and a doublet (e_g), with the latter lying lowest. A tetragonal distortion, caused by the Jahn–Teller effect, splits the e_g levels further, resulting in an orbital-singlet $d_{x^2-y^2}$ ground state. Consequently, it can be inferred that the Cu^{2+} ion substitutes at the $[Zr, Ti]^{4+}$ site, acting as an electron acceptor. The similarity of effective ionic radii between Ti^{4+} at 68 pm, Zr^{4+} at 81 pm and Cu^{2+} at 72 pm as compared to Pb^{2+} with a radius of 124 pm supports this assignment. Charge compensation presumably is reached by the creation of oxygen vacancies.

compound		$g_{zz}, g_\parallel$	g_{yy}	$g_{xx}, g_\perp$	ν_{mw} [GHz]	
Cu:PZT 54/46	site 1	2.342		2.082	94–240	this work
	site 2	2.402	2.082	2.050		
	site 3	2.402	2.082	2.029		
$Cu:PbTiO_3$		2.340(1)		2.058(1)	9	[10]
$Cu:[Pb,La]TiO_3$		2.38		2.11	9.57	[11]
$Cu:PbTiO_3$		2.340		2.058	9.6	[12]
Cu:PZT 57/43	site 1	2.39		2.082	9.6	[12]
	site 2	2.01		2.30		
Cu:PZT 90/10		2.420	2.093	2.085	9.6	[12]
Cu:PLZT 8/65/35	site 1	2.385		2.0795	9.378	[13]
	site 2	2.19		2.19		

TABLE 1 Experimentally obtained principal values of the g and hyperfine tensors for 0.25 mol %-doped Cu:PZT 54/46 as compared to values for similar compounds [10–13], measured at different mw frequencies ν_{mw}

However, even the W-band spectrum gives no clear evidence for an additional copper centre of orthorhombic symmetry because the relevant spectral region is masked by Mn(II) signals, thus preventing an unambiguous identification of spectral structures expected for copper centres with slightly different g matrices. Different centres are expected because the MPB is being thought to consist of a mesoscopic mixing of tetragonal (t) and rhombohedral (r) phases. To prove this hypothesis, EPR spectra at a still higher Larmor frequency were taken. The corresponding 240-GHz EPR spectrum at 4 K is depicted in Fig. 2, clearly displaying additional spectral features. In order to confirm the assignment of these structures to canonical orientations of copper centres, EPR spectra were also taken at various intermediate Larmor frequencies. Using a normalized field axis for spectral representation (g-value plot), it was verified that two spectral features marked by an asterisk are not invariant with respect to a change in microwave frequency. This is only possible if spectral positions are not determined by a dominating g matrix. We therefore tentatively assign these lines to Fe^{3+} impurities, contributing resonance lines with positions determined by zerofield splitting.

First, a fit was performed (see Fig. 3) considering in addition to the axial centre only one additional orthorhombic centre with g values $g_{xx} = 2.029$ and $g_{yy} = 2.056$, adjusted to account for the two additional lines apart from the dominating contribution from the centre with an axial g matrix ($g_\perp = 2.082$). Second, the lines are alternatively attributed to high-field stationary points of two different orthorhombic centres ($g_{xx}^{(1)} = 2.029$, $g_{xx}^{(2)} = 2.050$) and identical $g_{yy} = 2.082$ values as shown in Fig. 4. A much better spectral fit is obtained with the latter model, for which reason only these values are listed in Table 1. We tentatively assign the second orthorhombic centre to a Cu^{2+} site in the proposed monoclinic phase [3]. Since this phase is known to be temperature dependent, at ambient temperature the second orthorhombic centre should vanish. However, at these temperatures EPR signals were too weak to be detected using the transmission set-up of the 240-GHz spectrometer.

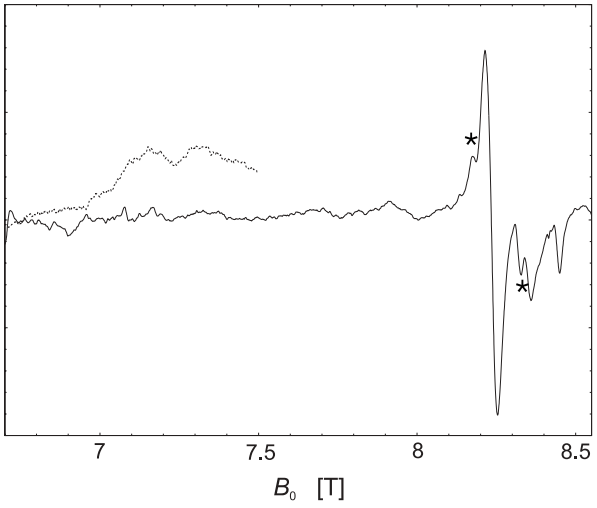

FIGURE 2 High-field EPR of 0.25 mol %-doped Cu:PZT 54/46 at $\nu_{mw} =$ 240 GHz and 4 K. The *inset* displays the low-field region recorded with increased signal to noise

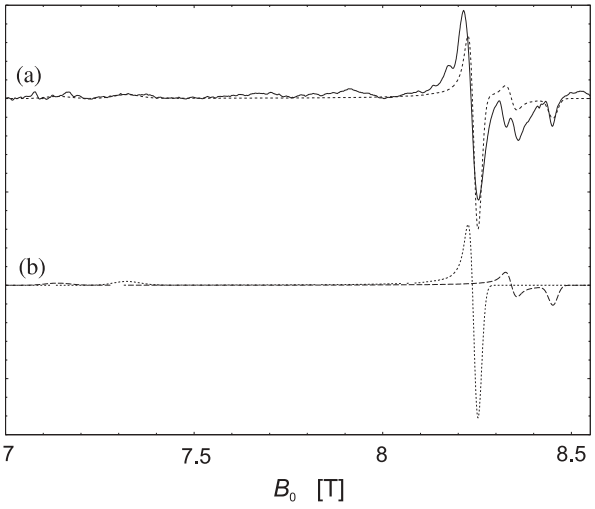

FIGURE 3 Least-squares fit of the experimental 240-GHz EPR spectrum (Fig. 2) invoking two simulated copper spectra of axial and orthorhombic symmetry. For details see text

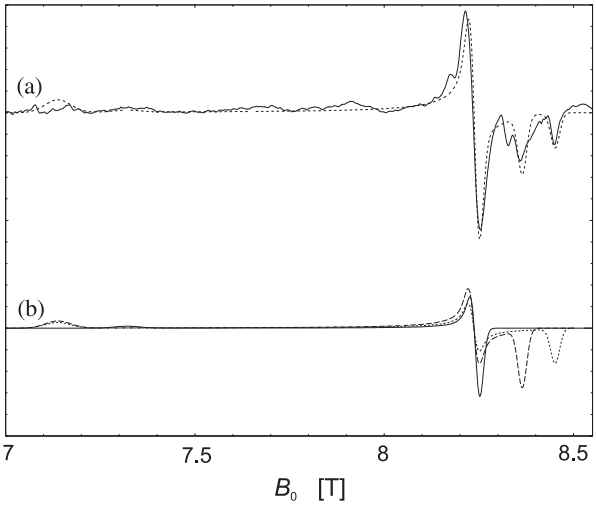

FIGURE 4 Least-squares fit of the experimental 240-GHz EPR spectrum (Fig. 2) invoking three simulated copper spectra, one of axial and two of orthorhombic symmetry. For details see text

At the low-field edge of the spectrum we could also resolve at least two spectral features (inset in Fig. 2). Since no direct assignment of the low-field features to particular axial and orthorhombic g-tensor components is possible, the X-band EPR data of Cu(II)-modified $PbTiO_3$ and PZT 90/10 (Table 1) are taken into account, for which $g_\parallel^{(t)} < g_{zz}^{(r)}$. This assumption is supported by the fact that the $g_\parallel$ and g_{zz} values generally are sensitive to a change in covalency of the $Cu^{2+}-O^{2-}$ in-plane π bonding [18, 19], which in turn is due to the $Zr^{4+}-O^{2-}$ bonding being more polar (ionic) than the $Ti^{4+}-O^{2-}$ bonding because of electronegativity differences.

The results obtained give evidence of an intrinsically heterogeneous compound, being consistent with either a superposition of high- and low-temperature rhombohedral phases or the proposed coexistence of a monoclinic phase [3], both of which give rise to a second orthorhombic g matrix. Therefore, at liquid-helium temperatures the MPB can be viewed as consisting of a mesoscopic mixing of three distinct phases. Utilizing the enhanced resolution of the high-field EPR spec-

tra, the relative amplitudes derived from the spectral fit in Fig. 4 allow for an estimation of the relative centre concentrations as 1 : 4 : 5 in the order axial : rhombohedral(1) : rhombohedral(2). This indicates a decrease of the tetragonal phase content as compared to X-ray data obtained at ambient temperature, showing a phase content of about 30%. Taking into account the proposed topology of the MPB, this observation agrees with the predicted tendency of a decreasing tetragonal phase content at lower temperatures.

On the basis of the observed, relatively broad EPR lines a considerable distribution of spin-Hamiltonian parameters (strain) has to be assumed, even though such variations are usually rather small in poly-crystalline materials as compared to glasses. Strain is generally due to variations of the local field around the $Cu^{2+}_{[Zr,Ti]}$ ion and may be particularly pronounced if the ion is preferentially located at grain boundaries, or if there are random electric fields or charge distributions in the ferroelectric material itself. Taking into account the results from ^{207}Pb-HYSCORE [15], the location at grain boundaries can be excluded. Furthermore, the charge-compensating oxygen vacancies were assigned to be situated at distant coordination spheres. It is thus supposed that local charge distributions due to charge compensation at distant spheres is responsible for the strain effects. An additional reason for the observed strain may be due to a varying ionicity of the $Cu^{2+}_{[Zr,Ti]}$–O^{2-} bonds in the octahedron, depending on Zr^{4+} or Ti^{4+} being the next nearest neighbour ions. The best-fit values for g strain, with FWHH of the Gaussian distributions $\delta g_{zz} = \delta g_{\parallel} = 0.005$, $\delta g_{xx} = \delta g_{yy} = \delta g_{\perp} = 0.0016$, were consistent with the observation that such random statistical distributions for Cu^{2+} systems are usually larger in the $g^{(t)}_{\parallel}$ and $g^{(r)}_{zz}$ orientations than perpendicular to this direction [20].

ACKNOWLEDGEMENTS This research has been financially supported by the DFG priority program 1051 'High-Field EPR in Biology, Chemistry and Physics' and centre of excellence 595 'Electrical Fatigue in Functional Materials'. The NHMFL is funded by the NSF through Grant DMR9016241. K.P.D. is grateful for a visiting professor fellowship at NHMFL.

REFERENCES

1 S.E. Park, T.R. Shrout: J. Appl. Phys. **82**, 1804 (1997)
2 H. Fu, R.E. Cohen: Nature **281**, 403 (2000)
3 B. Noheda, D.E. Cox, G. Shirane, J.A. Gonzalo, S.E. Park: Appl. Phys. Lett. **74**, 2059 (1999)
4 L. Bellaiche, A. Garcia, D. Vanderbilt: Phys. Rev. Lett. **84**, 5427 (2000)
5 R. Guo, L.E. Cross, S.E. Park, B. Noheda, D.E. Cox, G. Shirane: Phys. Rev. Lett. **84**, 5423 (2000)
6 D. Viehland: Phys. Rev. B **52**, 778 (1995)
7 X. Dai, J.F. Li, D. Viehland: J. Am. Ceram. Soc. **76**, 2815 (1995)
8 J. Ricote, D.L. Corker, R.W. Whatmore, S.A. Impey, A.M. Glazer, J.D.K. Roleder: J. Phys.: Condens. Matter **10**, 1767 (1998)
9 D.L. Corker, A.M. Glazer, R.W. Whatmore, A. Stallard, F. Fauth: J. Phys.: Condens. Matter **10**, 6251 (1998)
10 D.J. Keeble, Z. Li, M. Harmatz: J. Phys. Chem. Solids **57**, 1513 (1996)
11 O. Bidault, M. Actis, M. Maglione: Solid State Commun. **95**, 845 (1995)
12 W.L. Warren, B.A. Tuttle, F.C. Rong, G.J. Gerardi, E.H. Poindexter: J. Am. Ceram. Soc. **80**, 680 (1997)
13 Z. Bryknar, I.P. Bykov, M.D. Glinchuk, V.V. Laguta, Y.L. Maximenko, Z. Potuček, L. Jastrabik, H.-J. Schulz: Appl. Phys. A **66**, 555 (1998)
14 H.T. Langhammer, T. Müller, R. Böttcher, H.-P. Abicht: Solid State Sci. **5**, 965 (2003)
15 R.-A. Eichel, H. Kungl, M. Hoffmann: J. Appl. Phys. **95**, 8092 (2004)
16 A.K. Hassan, L.A. Pardi, J. Krzystek, A. Sienkiewicz, P. Goy, M. Rohrer, L.C. Brunel: J. Magn. Reson. **142**, 300 (2000)
17 (a) I. Yamada, M. Nishi, J. Akimitsu: J. Phys.: Condens. Matter **8**, 2625 (1996); (b) B. Pilawa: J. Phys.: Condens. Matter **9**, 3779 (1997); (c) W. Shentu, F. Lin, H. Hu: Phys. Chem. Glasses **39**, 130 (1998)
18 H. Imagawa: Phys. Status Solidi **30**, 469 (1968)
19 H. Hosono, H. Kawazoe, T. Kanazawa: J. Non-Cryst. Solids **33**, 103 (1979)
20 W. Froncisz, J.S. Hyde: J. Chem. Phys. **73**, 3123 (1980)